Available online at www.sciencedirect.com

ScienceDirect

Procedia Structural Integrity 33 (2021) 198–206

Structural Integrity Procedia

www.elsevier.com/locate/procedia

26th International Conference on Fracture and Structural Integrity

Setup of a numerical model for Post Welding Heat Treatment simulation of steel joints

Paolo Ferro[a]*, Filippo Berto[b], Roberto Meneghello[a]

[a]*University of Padova, Department of Engineering and Management, Stradella S. Nicola 3, 36100, Vicenza, Italy*
[b]*NTNU, Department of Engineering Design and Materials, Richard Birkelands vei 2b, 7491, Trondheim, Norway*

Abstract

A 3D numerical model aimed at predicting the deformations of a S355 steel T-joint in both as-welded and post-welding heat treated conditions was developed. Experimental tests were carried out with the objective to collect data necessary to the heat source calibration and model validation in terms of microstructure and joint distortions. All metallurgical phenomena were taken into account such as specific volume change and transformation plasticity induced by solid-state phase transformations. A viscoplasticity model for stress relief processing implemented in Sysweld finite elements code was used. Numerical results showed a satisfactory agreement with experimental ones. Further investigations will be necessary to consider also the validation of residual stress relief effects.

Keywords: Welding simulation; Stress relief heat trewatment; Steel; Distortions; Microstructure

1. Introduction

The S355J2 is a low carbon, high tensile strength structural steel of general use that finds application in the production of bridges, vehicles, ships, buildings, steel structures etc.. For this reason, it must be easily weldable, and its weldability is guarantee by its law carbon equivalent. Such steel is supplied in the normalized state and its impact

* Corresponding author. Tel.: +39 0444 998743; fax: +39 0444 998888.
E-mail address: paolo.ferro@unipd.it

2452-3216
10.1016/j.prostr.2021.10.024

energy at -20 °C is guaranteed to be at least 27J. Unfortunately, welding operations induce on the joints residuals stresses whose magnitude can approach the alloy's yield stress and cause a reduction of static and fatigue strength of the weldment at high cycle regime. For this reason, welded joints often undergo post welding heat treatments (PWHT) (Xie et al., 2015) aimed at reducing the residual stresses intensity and therefore increasing their mechanical properties (Thomas et al., 1993; Zhao et al., 1993). Stress relief heat treatments are widely carried out to improve the fatigue strength of steel welded joints in the high cycle fatigue regime where the effects of plasticity at the weld toe are negligible (Ferro and Berto, 2016; Ferro, 2014; Ferro and Petrone, 2009; Ferro et al., 2016; Ferro, 2012). Unfortunately, prediction of PWHT effects is not an easy task. Numerical simulation can be a formidable tool to reach that goal but, to the best of authors knowledge, it was not sufficiently explored in literature yet.

Zhang et al. (2018) used the instrumented indentation test and the microstructure-based finite element analysis to study the effect of post weld heat treatment on the mechanical properties of C-Mn weld metal. They found that the PWHT significantly influences the strength of weld metal by changing the strength of individual microstructures. Yaghi et al. (2020) developed a Finite Element (FE) model to predict the mitigating effect of PWHT on residual stresses in a circumferentially butt-welded P91 steel pipe, typically found as a structural component in steam pipelines in power plants. Because of the great number of welding passes (73) to weld a 55 mm thickness pipe wall, a 2D cross section model was used. Despite this simplification, a good agreement was found between experimental and numerical results in terms of residual stress. The Norton creep law was implemented in the model to simulate the stress relief phenomenon. The effects of PWHT on the residual stress (RS) and deformation of 20/0Cr18Ni9 dissimilar metal welded joint were studied by Huang et al. (2020) by means of experimental and numerical analyses. They found that the heat treatment temperature has the greatest effect on the reduction of residual stress and deformation, and the reduction of residual stress is also affected by the plasticity of the material. Finally, the electron beam welding and post welding heat treatment coupling simulation of GH80A plates was performed by Hong et al. (2018) using ABAQUS. Again, the Norton creep law (Stouffer and Dame, 1996) was implemented in the model for the PWHT simulation.

Despite the great interest in models related to PWHT simulation, in view of the prediction of fatigue strength improvement coming from stress relief, no sufficient literature was found on this topic and in particular when the common structural steel S355 is considered. Therefore, this work is aimed at filling this gap. Computational welding mechanics was used to simulate a T-joint welding process (Ferro et al., 2005) using only one pass on one side only. A kinematic creep law, implemented in Sysweld numerical code, was used to model the stress relief phenomenon.

The model was validated through the experimental measurement of the distortion angle between the flange and the web before and after PWHT.

2. Materials and Methods

The analyzed material is the structural carbon steel S355J2+N, whose chemical composition is summarized in Table 1.

Table 1. Chemical composition (wt%) of the analyzed steel

C	Mn	Si	P	S	Cr	Ni	Mo	Cu	Sn	Al	CEV
0.19	1.23	0.029	0.008	0.0024	0.0686	0.0638	0.0098	0.1930	0.0143	0.0298	0.4281

Square groove T joints were obtained by arc welding a 5 mm thick web (200x100 mm) on a 5 mm thick flange (200x200 mm) using a single pass on only one side as schematized in Fig. 1a.

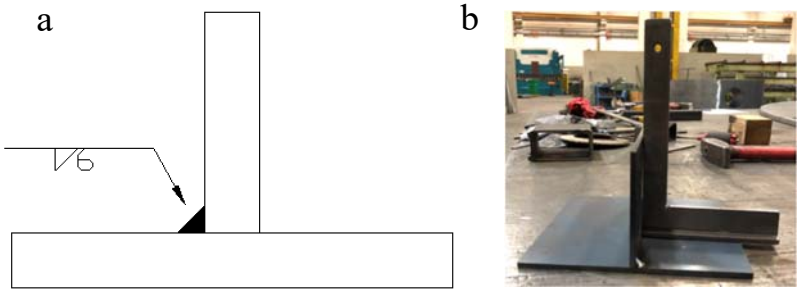

Fig. 1. (a) Schematic of the T joint, (b) accurate plates positioning before welding

Prior welding, the plates were stress relieved at 300 °C for 1.5h in order to avoid unexpected deformations during joining operations. Moreover, the flange and the web were tack welded and perfectly positioned perpendicularly to each other using a square (Fig. 1b). Table 2 summarizes the parameters used in the manual gas metal arc welding (GMAW) process used in this work.

Table 2. GMAW parameters

Fille wire diameter [mm]	Shielding Gas	Potential (Volt)	Current (A)	Fille wire speed [mm/s]	Welding speed [mm/s]
1.2	Ar 92%-CO_2 8%	29.8	290	8.7	5.8

The measurement of the joints distortions before and after the stress relief heat treatment (510 °C, 3h) was performed using an absolute arm and a support to keep the samples in position during the measurements. The obtained points cloud was then elaborated via software to obtain the angle between the web and the flange as shown in Fig. 2. Results are summarized in table 3.

Table 3. Angle between the web and the flange (weld side)

Joint condition	Sample number	Angle (°)	Deformation (°)
As-welded	1	88.41	1.59
	2	88.48	1.52
	3	88.32	1.68
	4	88.75	1.25
	5	88.71	1.29
	6	88.68	1.32
Stress-relieved	1	88,41	1.59
	2	88.32	1.68

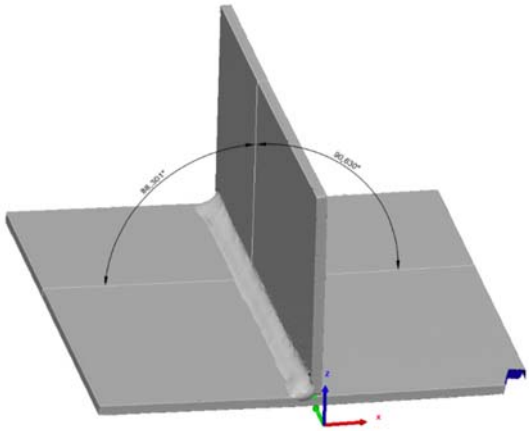

Fig. 2. Angle measurement via software

It is noted that, despite the manual welding operations, a confident distortion angle in the as-welded condition was obtained with a mean value of 1.44° ± 0.17°. Moreover, the stress relief heat treatment didn't modify the deformation angle (Tab. 3). Finally, standard metallographic analyses, using the optical microscope Leica LM2500, were carried out to investigate the microstructure of the weld.

2. Numerical model

2.1. Welding simulation

The welding simulation was carried out by the numerical code Sysweld®. The mesh, shown in Figure 3, consists of 64384 8-node brick elements. In order to take into account the effect of filler metal, a groups of elements modeling the throat were created. By referring to Figure 3, the white elements belong to the parent metal and are always active during simulation; the bleu ones define the filler metal and are activated during welding. Thermo-metallurgical and mechanical properties of both filler and parent metals were taken from Sysweld database. In the present analysis, the following microstructural constituents were considered: martensite, bainite, ferrite-pearlite, tempered martensite, tempered bainite and austenite. They were modeled by means of the Leblond-Devaux (1984) and Koistinen-Marburger (1959) equations according to their diffusional or non-diffusional feature. The simplifying assumptions were made that tempered bainite has the same properties as ferrite and that tempered martensite is similar in properties to bainite.

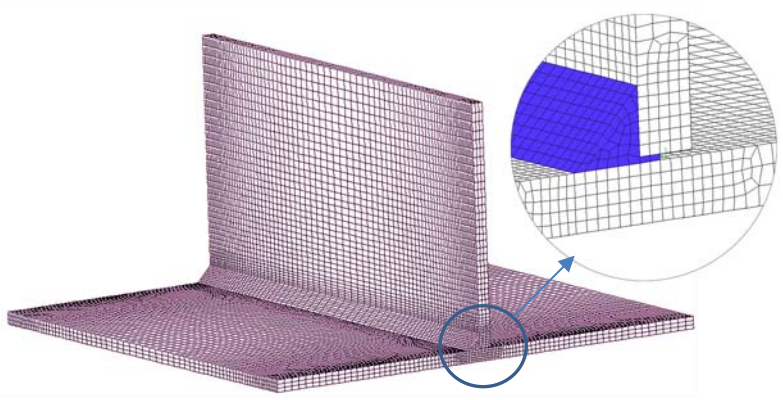

Fig. 3. Mesh of the T-joint with highlighted in bleu the elements group modelling the filler metal

The heat source was modeled using a double ellipsoid power density distribution function proposed by Goldak et al. (1984) (Eq. 1) that has been used previously in literature for arc welding simulation (Ferro et al., 2010).

$$\begin{cases} q_F = \dfrac{6\sqrt{3}f_f Q_W}{abc_f\pi\sqrt{\pi}} \exp\left(\dfrac{-3x^2}{a^2}\right)\exp\left(\dfrac{-3y^2}{b^2}\right)\exp\left(\dfrac{-3z^2}{c_f^{\,2}}\right) & \text{source front} \\ q_R = \dfrac{6\sqrt{3}f_r Q_W}{abc_r\pi\sqrt{\pi}} \exp\left(\dfrac{-3x^2}{a^2}\right)\exp\left(\dfrac{-3y^2}{b^2}\right)\exp\left(\dfrac{-3z^2}{c_r^{\,2}}\right) & \text{source rear} \end{cases} \quad (1)$$

In previous expressions (1), q_F and q_R represent the frontal and rear power density, respectively; Q_W is the welding heat input estimated from the input current (I) and voltage (V) parameters ($QW=\eta VI$, with η the thermal efficiency set for GTAW equal to 0.8); f_f(= 0.6) and f_r (= 1.4) denotes the fractions of heat present in the front and rear parts of the heat source, while a, b, c_f and c_r are Gaussian parameters of the Goldak's heat source that were chosen in a way that it produces a proper molten weld pool. All Goldak's heat source parameters adopted in the FE analyses have been summarized in Table 4.

Table 4. Goldak's heat source parameters used in the simulation

Q (=VI) [W]	a [mm]	b [mm]	c_f [mm]	c_r [mm]	v [mm/sec]
8642	5.5	5.5	4.5	9	5.8

The molten effect was simulated by incorporating a function that clears the history of an element once the temperature exceeds the melting temperature, which was taken as 1536°C. Radiative heat loss (using the Stephan-Boltzmann law) and convective heat loss (using a convective heat transfer coefficient equal to 25 W/m^2K) were applied at the boundary (external surfaces) of the plates to be joined. In the mechanical computation the weldment was considered isostatically clamped. Finally, a sequentially coupled thermo-metallurgical and mechanical analysis was performed.

2.2. Heat treatment simulation

After welding simulation, the joint underwent the furnace thermal history used to carry out the experimental stress relief heat treatment. In the mechanical computation the viscous plastic deformation (ε^p) of the alloy was modeled by using the following creep law (kinematic approach):

$$\dot{\varepsilon}^p = K\left(\sigma - \frac{3}{2}\alpha\right)^n \tag{2}$$

$$\dot{\alpha} = H\dot{\varepsilon}^p - \left(\frac{3}{2}\right)^{P-1} C\alpha^P \tag{3}$$

where α is the kinematic strain-hardening variable and H, K, C, P and n are temperature dependent constants (Table 5). The term $H\dot{\varepsilon}^p$ describes the strain hardening and $-(3/2)^{P-1}C\alpha^P$ corresponds to viscous recovery. Primary creep corresponds to the commencement of the experiment, when α has reached its static state (obtained by cancelling $\dot{\alpha}$ in equation (3), the value of $\dot{\varepsilon}^p$ being less than that for primary creep). Secondary creep therefore results, in this model, from a state of equilibrium between strain hardening and viscous recovery. This corresponds to physical reality.

Table 5. Creep law parameters as a function of Temperature

T [°C]	$\log_{10}$(K)	n	H	$\log_{10}$(C)	P
400	-80	1	10	-1	1
482	-15.555	3.4	85000	-12.511	4
565	-15	4.11	29040	-15.511	7
650	-11.523	3.2	12000	-6.2218	1.9

3. Results and discussion

3.1. Thermo-metallurgical results

Fig. 4 shows some results of the temperature computation. The fusion zone dimension and shape are in sufficient good agreement with that obtained in the experiments. Metallurgical results and comparinon with experiments are summarized in Fig. 5. The FZ microstructure consists of acicular and Widmanstätten ferrite with islands of allotriomorphic ferrite, in agreement with the microstructure observed in low carbon steels welded joints (Babu, 2004). In the range between 800-300 °C the austenite decomposes to different ferrite morphologies. The austenite to ferrite decomposition starts with the formation of allotriomorphic ferrite at the prior γ–γ boundaries. With continued cooling, the Widmanstätten ferrite nuclease at ferrite/austenite boundaries and extends into the untransformed austenite-grain interiors. With further cooling to low temperatures, the acicular ferrite would nucleate on the inclusion. If there are no inclusions, bainitic ferrite might form instead of acicular ferrite, from the remaining austenite. The heat affected zone (HAZ) of the as-welded joint was mainly composed of bainite.

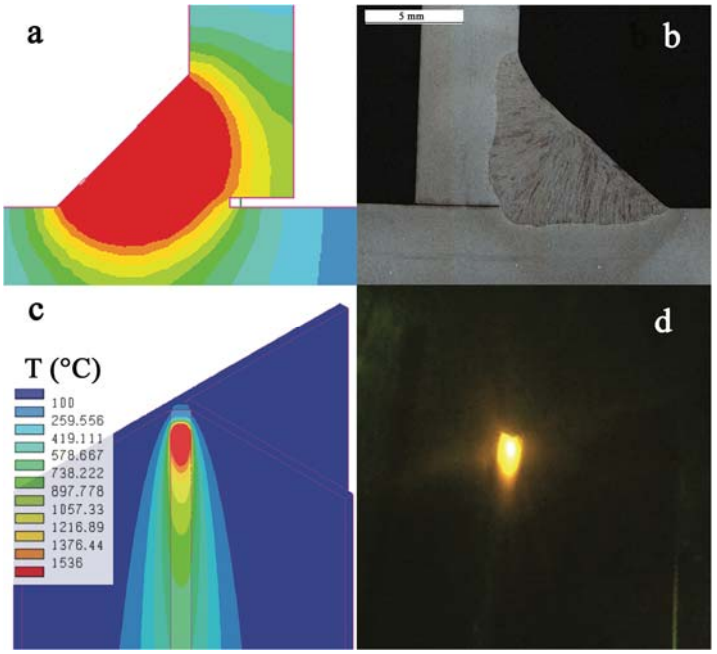

Fig. 4. (a,c) results of temperature computation and comparison with experimental observations (b,d).

All these microstructural features were found in good agreement with those predicted by the model (Fig. 5)

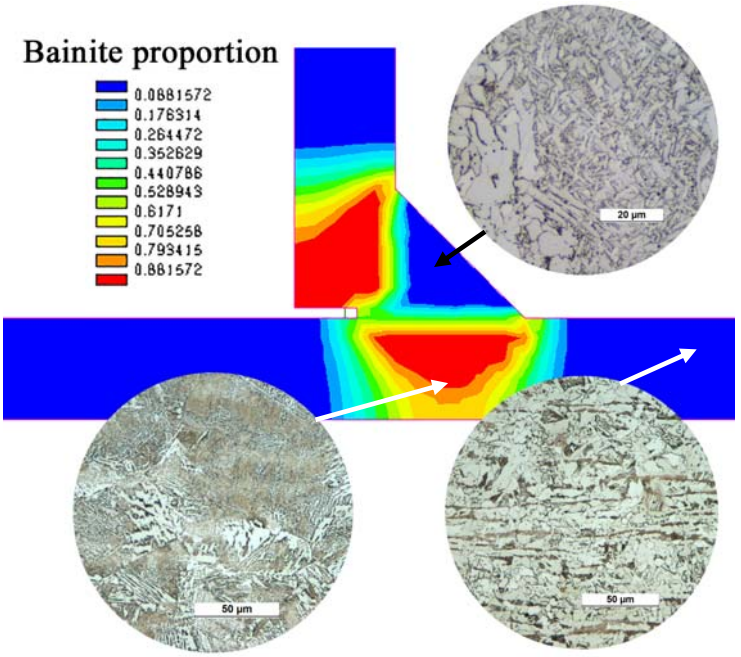

Fig. 5. Metallurgy of the joint in the as-welded condition.

3.2. Mechanical results

After welding the angle between the flange and the web obtained by the numerical model was 88.80 ° against an experimental value of 88.56± 0.17° that is a reasonable good result, given the complexity of the process modelled and the order of magitude of the deformed shape. Fig. 6 shows the deformed shape of the T-joint afeter welding.

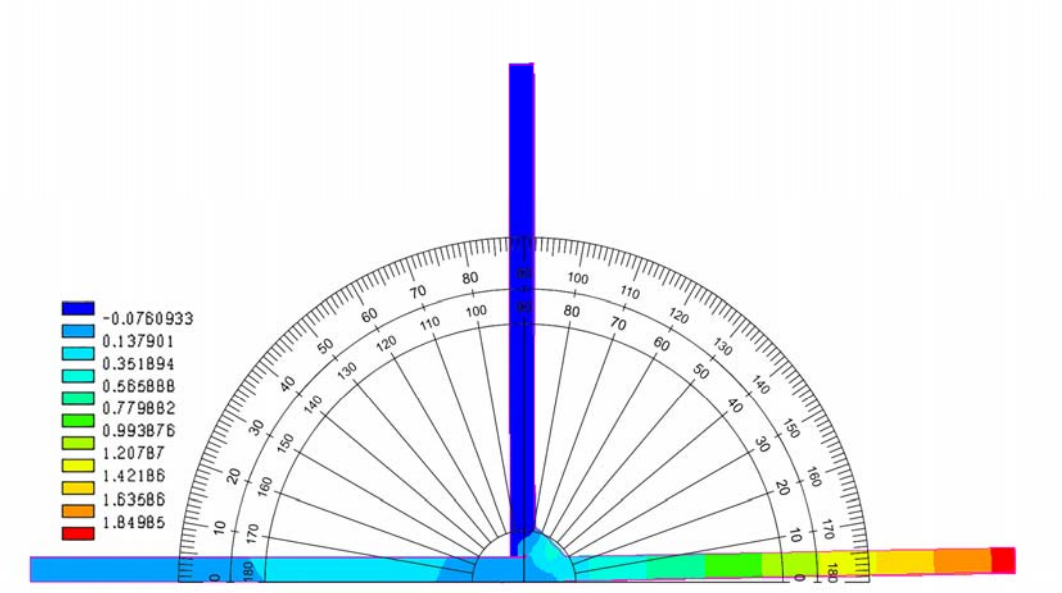

Fig. 5. Nodes displacement U_y.

After stress relief heat treatment, the distortion angle didn't show any variation and the numerical results confirmed that experimental evidence. However, residual stress reduced significantly as shown in Fig. 6.

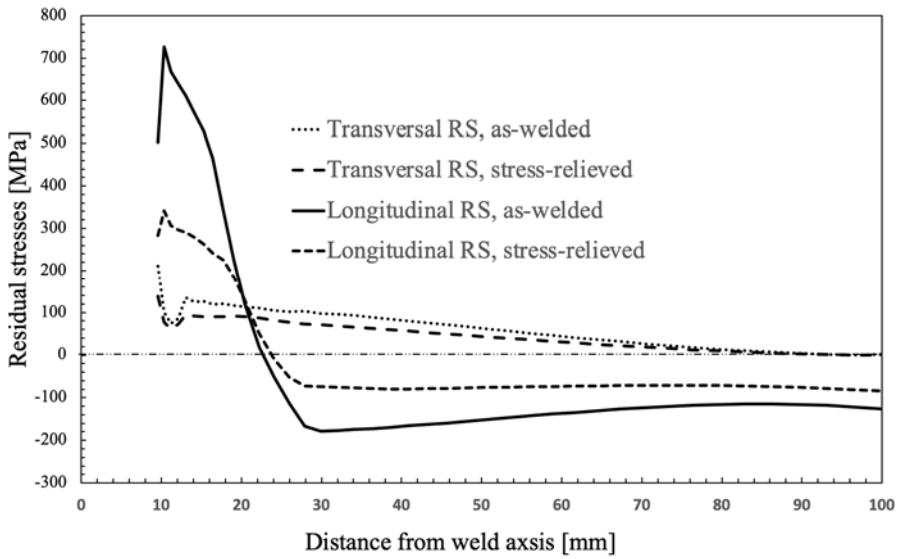

Fig. 6. Residual stress along upper surfece of the middle cross section starting from the weld toe.

4. Conclusions

A preliminary setup of a numerical model aimed at predicting the deformation and residual stress before and after post welding heat treatment of structural steels was successfully caried out. The main phenomena involved in the welding process and heat treatment were taken into account with particular attention to solid state phase transformation effects. A creep kinematic law was implemented and applied to predict the mechanical effects of the stress relief heat treatment. Results showed a good agreement between the numerical and experimental results in terms of both microstructure and welding induced distortions. Further investigations are in progress to validate also the residual stress relief prediction.

References

Babu, S.S., 2004. The mechanism of acicular ferrite in weld deposits. Current Opinion in Solid State and Materials Science 8, pp. 267-278.

Ferro, P. and Berto, F. 2016. Quantification of the influence of residual stresses on fatigue strength of Al-alloy welded joints by means of the local strain density approach. Strength of Materials 48(3), 426–436.

Ferro, P., 2012. The influence of phase transformations on the asymptotic residual stress distribution arising near a sharp V-notch tip. Modelling Simul. Mater. Sci. Eng. 20(8), 085003.

Ferro, P., 2014. The local strain energy density approach applied to pre-stressed components subjected to cyclic load. Fatigue Fract Eng Mater Struct 37, 1268–1280.

Ferro, P., Berto, F. and James, N.M., 2016. Asymptotic residual stresses in butt-welded joints under fatigue loading. Theoretical and Applied Fracture Mechanics 83, 114–124.

Ferro, P., Bonollo, F., Tiziani, A., 2005. Laser welding of copper-nickel alloys: A numerical and experimental analysis. Science and Technology of Welding and Joining 10(3), 299-310.

Ferro, P., Bonollo, F., Tiziani, A., 2010. Methodologies and experimental validations of welding process numerical simulation. Int J Computational Materials Science and Surface Engineering 3, 114-32.

Ferro, P., Petrone, N., 2009. Asymptotic thermal and residual stress distributions due to transient thermal loads. Fatigue and Fracture of Engineering Materials and Structures 32(11), 936-948.

Goldak, J., Chakravarti, A. and Birbby, M., 1984. A new finite element model for welding heat sources. Metallur Trans B 15b, 299–305.

Hong, Z., Zhengxing, M., Jiukai, L., Yongjie, L., Qingyuan, W., 2018. Numerical Simulation of the Electron Beam Welding and Post Welding Heat Treatment Coupling Process. High Temp. Mater. Proc. 37(9-10), 793–800.

Huang, B., Liu, J., Zhang, S., Chen, Q., Chen, L., 2020. Effect of post-weld heat treatment on the residual stress and deformation of 20/0Cr18Ni9 dissimilar metal welded joint by experiments and simulations. J. Mater. Res. Technol. 9(3), 6186-6200.

Koistinen, D.P. and Marburger, R.E., 1959. A general equation prescribing extent of austenite-martensite transformation in pure iron-carbon alloys and carbon steels. Acta Metall 7, 59-68.

Leblond, J.B. and Devaux, J., 1984. A new kinetic model for anisothermal metallurgical transformations in steels including the effect of austenite grain size. Acta Metall 32, 137-46.

Stouffer, D.C. and Dame, L.T.,1996. Inelastic Deformations of Metals: Models, Mechanical Properties and Metallurgy, John Wiley and Sons Ltd, New York (1996).

Thomas, G., Ramachandra, V., Ganeshan, R., Vasudevan, R., 1993. Effect of pre- and post- weld heat treatments on the mechanical properties of electron beam welded Ti-6Al- 4V alloy, J. Mater. Sci. 28, 4892–4899.

Xie, P., Zhao, H., Wu, B., Gong, S., 2015. Evaluation of residual stresses relaxation by post weld heat treatment using contour method and X-ray diffraction method, Exp. Mech. 55, 1329–1337.

Yaghi, A.H. et al., 2020. Comparison of measured and modelled residual stresses in a welded P91 steel pipe undergoing post weld heat treatment. International Journal of Pressure Vessels and Piping 181, 104076.

Zhang, C., Yang, S., Gong, B, Deng, C., Wang, D., 2018. Effects of post weld heat treatment (PWHT) on mechanical properties of C- Mn weld metal: Experimental observation and microstructure-based simulation. Materials Science & Engineering A 712 (2018) 430–439.

Zhao, M.S., Chiew, S.P., Lee, C.K., 2016. Post weld heat treatment for high strength steel welded connections, J. Constr. Steel Res. 122, 167–177.